Title

Subtitle

by

Mikkel Metzsch Jensen

THESIS

for the degree of

MASTER OF SCIENCE

Faculty of Mathematics and Natural Sciences
University of Oslo

Spring 2023

Title

Subtitle

Mikkel Metzsch Jensen

Abstract

Abstract.

Acknowledgments

Acknowledgments.

iv

Contents

List of symbols?

Maybe add list of symbols and where they are used like Trømborg.

Chapter 1

Background Theory and Method

Small introtext to motivate this chapter. What am I going to go over here.

1.1 Tribology - friction

1.1.1 Friction on a macroscopic scale - macroscale theories

1.1.1.1 Amontons' law.

The work of Leonardo da Vinci (1452–1519), Guillaume Amontons (1663-705) and Charles de Coulomb (1736-1806) all contributed to what is commonly known as Amontons' law describing the frictional force accuring when starting and keeping a solid block sliding against a solid surface. This emperical law states that the frictional force tangential to the sliding direction is entirely independent of contact area and sliding velocity (at ordinary sliding velocities). Instead it relies only on the normal force F_N acting from the surface on the block and the material specific friction coefficient μ as

$$F_f = \mu F_N.$$

Further it distinguish between *static* and *kinetic* friction as the cases of stationary and sliding contact resepectively. Each type of friction comes with its own friction coefficient, μ_s for static and μ_k for kinetic friction, usually with values lower than one and $\mu_s \geq \mu_k$ in all cases. [1][p. 6].

This simple law is a natural starting point for the
Allthough this model is a common base for understanding friction on a macroscopic level is has its limitations. It turns out that static friction is not constant, but depends on the so-called contact history with increasing friction as the logarithm of time of stationary contact [2]. For the kinetic friction the independency of sliding velocity dissapears at low velocities as thermal effects becomes important and for high velocities due to intertial effetcs. [1][pp. 5-6].

It fails to explain the mechanisms behind fritction.
In order to understand what is causing friction between moving objects and how this might result in a linear relationship between friction and normal force we must take the study to a smaller scale... Having an emperical law that seems to predict the friction in many cases leads to the next natural desire for deriving these from fundamental atomic or molecular principles.

1.1.2 Friction on a microscopic scale - Nanotribology

It is generally accepted that friction is caused by two mechanism: mechanical friction and chemical friction. The mechanical friction is the plowing of the surface by hard particles or asperities. The chemical mechanism is adhesion between contacting surfaces. [3].
Sources in general: [4], [3]

1.1.2.1   Surface roughness - Asperity theories

Going beyond a macroscopic perspective we realise that most surfaces is in fact rough. The contact between two surfaces consist of numerous smaller contact point, so-called asperities, each with a contact area of A_{asp}. The true contact area $\sum A_{\text{asp}}$ is found to be much smaller than the apperent macroscopic area A_{macro}. The friction force is shown to be proportional (extra source on this) to this true contact area as

$$F_f = \tau \sum A_{\text{asp}},$$

where τ is an effective shear strength of the contacting bodies. This is still compatible with Amontons' law as long as we differenciate between the macroscopic macroscopic and true area and by having the true contact area dependt linearly on applied normal force.

Thus many studies have focused individual asperities to reveal the relationship between the contact area and normal force (13-15 from [4]). By assuming perfectly smooth asperities with radii of curvature from nanometers to micrometres in size continuum mechanics can be used to predict the deformation of asperities as normal force is applied. A model for non-adhesive contact between homogenous, isotropic, linear elastic spheres was first developed by Hertz (17 [4]), which predicted $A_{\text{asp}} \propto F_N^{2/3}$. Later adhesion effects were included in a number of subsequent models, including Maugis-Dugdale theory (18 from [4]), which also predicts a sublinear relatinship between A_{asp} and f_N leading to a similar sublinear relationship for F_f and F_N.
[4].

1.1.2.2   Atomic level friction

On the smallest possible scale, atomic scale, the surfaces does not have structural asperities. Instead atomic level friction is being model as a consequencse of the rough potential of the atomic landscape.

1.1.2.3   Frenkel-Kontorova-Tomlinson (FKT)

Describes atomic scale friction (not fully accurately though) and gives insight in stick slip motion.

1.1.2.4   Commensurate and incommensurate

1.1.2.5   Stick slip

At nanoscales things get a bit more unclear. SFM (explain) experiments have reported (copy sources 5, 6, 21 from [4]) where $F_f \propto F_N$ or even with these quantities being nearly independent of each other.
In several works by J. Fineberg's group [2–4] the transition from sticking to sliding is characterized by slip fronts propagating along the interface. [5][p. 2].

1.1.2.6   Commensurate and incommensurate

As expected, high levels of friction were present in the commensurate positions and extremely low friction was found when the surfaces were incommensurate. (https://physicsworld.com/a/friction-at-the-nano-scale/)

1.1.2.7   Superlubricity?

Superlubricity, now a pervasive concept of modern tribology, dates back to the math- ematical framework of the Frenkel Kontorova model for incommensurate interfaces [40]. When two contacting crystalline workpieces are out of registry, by lattice mismatch or angular misalignment, the minimal force required to achieve sliding, i.e. the static friction, tends to zero in the thermodynamic limit – that is, it can at most grow as a power less than one of the area – provided the two substrates are stiff enough. (Current trends in the physics of nanoscale friction)
Superlubricity is experimentally rare. Until recently, it has been demonstrated or im- plied in a relatively small number of cases [29, 42–46]. There are now more evidences of superlubric behavior in cluster nanomanipulation [32, 33, 47], sliding colloidal layers [48–50], and inertially driven rare-gas adsorbates [51, 52]. (Current trends in the physics of nanoscale friction)

A breakdown of structural lubricity may occur at the heterogeneous interface of graphene and h-BN. Because of lattice mismatch (1.8%), this interface is intrinsically incommen- surate, and superlubricity should persist regardless of the flake-substrate orientation, and become more and more evident as the flake size increases [57]. However, vertical cor- rugations and planar strains may occur at the interface even in the presence of weak van der Waals interactions and, since the lattice mismatch is small, the system can de- velop locally commensurate and incommensurate domains as a function of the misfit angle [58, 59]. Nonetheless, spontaneous rotation of large graphene flakes on h-BN is observed after thermal annealing at elevated temperatures, indicative of very low friction due to incommensurate sliding [60, 61]. (Current trends in the physics of nanoscale friction)

Indeed, we know from theory and simulation [74–76] that even in clean wearless friction experiments with perfect atomic structures, superlubricity at large scales may, for example, surrender due to the soft elastic strain deformations of contacting systems. (Current trends in the physics of nanoscale friction)

1.1.3 Temperature dependence

Thus, it is commonly expected that the friction of a dry nanocontact should classically decrease with increasing temperature provided no other surface or material parameters are altered by the temperature changes [77, 80–83]. (Current trends in the physics of nanoscale friction)

1.1.4 Summary of expected frictional properties

1. Friction should decrease by increasing temperature.

2. We expect stick slip motion

3. What about dependence on normal force?

4. Dependence on contact area?

5. Dependense on speed?

- Different friction models on macro-and microscopic scale

1.1.5 Graphene friction

Theory of friction experiment involving graphene.

Because of this frictional reduction, many studies indicate graphene as the thinnest solid-state lubricant and anti-wear coating [104–106]. (Current trends in the physics of nanoscale friction)

Accurate FFM measurements on few-layer graphene systems show that friction decreases by increasing graphene thickness from a single layer up to 4-5 layers, and then it approaches graphite values [97, 99, 101, 107, 108]. (Current trends in the physics of nanoscale friction)

1.2 Molecular Dynamics

- MD simulation (classical or ab initio)

- Basics of classical MD simulations: Integration and stuff

- Ab initio simulation (quantum mechanics, solving schrödinger)

1.2.1   Potentials

The choices of potentials used in the MD simulation is mainly based on the on [6] which have a somewhat similar MD friction simulation, the difference being that they impose a Si-tip on the graphene sheet supported by a Si-substrate where we impose drag the whole sheet upon the substrate. Nonetheless this serves as a good anchor for the methodology of the setup. The covalent bonds of C-C in graphene and Si-Si in the substrate is described by the Tersoff and Stillinger–Weber potentials, respectively. A typical 12-6 Lennard–Jones potential is used to describe the van der Waals adhesive interaction between graphene and the substrate.

1.2.1.1   General formulation of potentials...?

On a general note we can generalize the n-body potential as the expansion in orders of participating atoms as

$$E = \sum_i V_1(\mathbf{r}_i) + \sum_{\substack{i,j \\ i<j}} V_2(\mathbf{r}_i, \mathbf{r}_j) + \sum_{\substack{i,j,k \\ i<j<k}} V_3(\mathbf{r}_i, \mathbf{r}_j, \mathbf{r}_i) + \cdots .$$

where $\mathbf{r}_n$ is the position of the nth particle and V_m is called an m-body potential [7]. The first one-body term corresponds to an external potential, followed by the two-body term, the three-body term and so on.The simplest model that includes parrticle interaction is the pair potential truncating the expansion after the two-body term. A general feature of the pair potentials is that they favor close-packed structures which is unsuited to describe covalent bonds that take more open structures. In particular, pair potentials are completely inapplicable to strongly co- valent systems such as semiconductors [7]. In order to accomodate the description of covalent bonds the natural step is thus to include the next step of the expansion, the three-body terms, as we will see for the modeling of the graphene sheet C-C bonds and the Silicon sheet Si-Si bonds. For the interaction between the sheet and the substrate we can nøjes med a Lennard Jones pair potential describing the non-bonded van der Waals interaction.

1.2.2   Lennard Jones

This sections is based on [[8], [9], [10]].

    The Lennard-Jones (LJ) model is probably one of the most famous pair potentials used in MD simulations. LJ models the potential energy between two non-bonding atoms based solely on interatomc distance r. The model accounts for attractive forces arising from dipole-dipole, dipole-induced dipole and London interactions, and repulsive forces that capture the hard core (is this safe to say?) of overlapping wave functions at small distances. Thus it is assummes neutrally charged atoms and was orginally proposed for noble gases. The classical 12-6 version of the model (refering to the power law of the repulsive and attractive forces respectively) reads

$$E = 4\epsilon \left[\left(\frac{\sigma}{r} \right)^{12} - \left(\frac{\sigma}{r} \right)^6 \right], \qquad r < r_c, \tag{1.1}$$

where r is the interatomic distance with cut-off r_c, ϵ is the depth of the potential well and σ the distance where the potential is zero. By solving for the potential minimum ($dE/dr = 0$) we find the equilibrium distance to be $r_0 = \sigma 2^{1/6}$. This makes for an even cleary interpration of σ which effectively sets the equilirbium distance between atoms, i.e. the dividing line for which the net force is repulsive or attractive. While the LJ model in many ways is an oversimplified model that is insufficient in its description of ... (get source and concrete examples) it is commonly used as a model for intermaterial interactions (between moving object and substrate) in friction studies [[6], [11], [3]].

1.2.3   Stillinger weber

This section is based on [[12], [13]]

    The stillinger weber potential takes the form of a three body potential

$$E = \sum_i \sum_{j>i} \phi_2(r_{ij}) + \sum_i \sum_{j \neq i} \sum_{k>j} \phi_3(r_{ij}, r_{ik}, \theta_{ijk}),$$

where r_{ij} denotes the distance between atom i and j and θ_{ijk} the angle between bond ij and jk. The summations is over all neighbours j and k of atom i within a cut-off distance $r = a\sigma$.
The two-body term ϕ_2 builds from the LJ model with the addition of an exponetial cutoff term

$$\phi_2(r_{ij}) = A_{ij}\epsilon_{ij}\left[B_{ij}\left(\frac{\sigma_{ij}}{r_{ij}}\right)^{p_{ij}} - \left(\frac{\sigma_{ij}}{r_{ij}}\right)^{q_{ij}}\right]\exp(\frac{\sigma_{ij}}{r_{ij} - a_{ij}\sigma_{ij}}). \tag{1.2}$$

The model parameters A, ϵ, B, σ, p, q and a comes with i, j indices to indicate that theese parameters should be specified for each unique pair of atom types. However, in our case we will only provide a single value for each model parameter as we are exclusively dealing with Si-Si bonds. We see that the first term in eq. (1.2) is reminiscent of the LJ model in eq. (1.1) while the last term effectively drives the potential to zero at $r = a\sigma$, which is thus the chosen cut-off distance for the potential evaluation. With the model parameters for the Si-Si modelling (see table 1.1) the cut-off becomes ~ 3.8 Å.
The three body term includes an angle dependency as

$$\phi_3(r_{ij}, r_{ik}, \theta_{ijk}) = \lambda_{ijk}\ \epsilon_{ijk}\left[\cos\theta_{ijk} - \cos\theta_{0,ijk}\right]^2\exp(\frac{\gamma_{ij}\sigma_{ij}}{r_{ij} - a_{ij}\sigma_{ij}})\exp(\frac{\gamma_{ik}\sigma_{ik}}{r_{ik} - a_{ik}\sigma_{ik}}), \tag{1.3}$$

where $\theta_{0,ijk}$ is the equilibrium angle. The first term of eq. (1.3) includes an angle dependency analog to a harmonic oscillator based on a cosine angle distance from the equilibrium angle. The final two terms act again as a cut-off function by driving the potential to zero at $r_{ij} = a_{ij}\sigma_{ij}$ and $r_{ik} = a_{ik}\sigma_{ik}$ respectively.
The parameters used for the Si-Si bond modeling is displayed in table 1.1 along with an interpretation of each model parameter.

Table 1.1: Parameters for the stilliner weber potential used for intermolecular interactions in the silicon substrate.

Parameter	Value	Description
ϵ	2.1683	Individual depth of the potential well for each atom type pair/tiplets.
σ	2.0951	Distance for which the individual pair interactions has zero potential (analog to the LJ model).
a	1.80	The individual cut-off distance for each atom type pair.
λ	21.0	The overall depth of the three-body potential well.
γ	1.20	The shape of the three-body cut-off terms.
$\cos(\theta_0)$	-1/3	Cosine of equilibrium angle.
A	7.049556277	The overall depth of the two-body potential well.
B	0.6022245584	Scales the repulsion part of the two-body term.
p	4.0	The power dependency for the repulsion part of the two-body term.
q	0.0	The power dependency for the attraction part of the two-body term.
tol	0.0	LAMMPS: Option to define a different cut-off than the theoretical of $r = a\sigma$. $tol = 0$ refers to the theoretical being used.

1.2.4 Tersoff

This section is based on [[14], [7]].
The tersoff potential abandon the idea of a general n-body form and attempts instead to build the model on a more physics informed approach; The more neighbours an atom has the weaker the bonds will be. Thus it introduces the bond order (bond strentgh), that is environment specific and decrease with increasing bond coordination (number of neighbours for a given atom). The potential energy is taken to have the form

$$E = \sum_i E_i = \frac{1}{2}\sum_{i\neq j}V_{ij},$$
$$V_{ij} = f_C(r_{ij})\left[f_R(r_{ij}) + b_{ij}f_A(r_{ij})\right],$$

where the total potential energy is decomposed into a bond energy V_{ij}. The indices i and j run over the atoms of the system with r_{ij} denoting the distance between atom i and j. Notice that the sum includes all combinations of i, j where $i \neq j$ meaning that the same bond is double counted which is the reason for the additional factor $1/2$. The reasoning behind comes from the asymmetry of the bond order $b_{ij} \neq b_{ji}$ leading to a $V_{ij} \neq V_{ji}$. The bond energy is composed of a repulsive term f_R, arising from overlapping wave functions, and an attractive term f_A associated with bonding. f_c is simply a smooth cut-off function to increase computational efficiency. b_{ij} represent the bond order, i.e. the strength of the bonds, which depends inversely on the number of bonds, the bond angles (θ_{ijk}) and optionally the relative bonds lengths (r_{ij}, rjk). Notice that an additional cut-off term a_{ij} was orginally multiplied to f_R as a way of including terms that limit the range of the interactions to the first neighbour shell. These kind of limitations is already included in b_{ij} for the attractive term f_A but is often omitted for the repulsive term f_R, and we do so to by setting $a_{ij} = 1$.

The cut-off function f_C goes from 1 to 0 over a small interval range $R \pm D$ as

$$f_C(r) = \begin{cases} 1 & r < R - D \\ \frac{1}{2} - \frac{1}{2}\sin\left(\frac{\pi}{2}\frac{r-R}{D}\right) & R - D < r < R + D \ , \\ 0 & r > R + D \end{cases}$$

which is continuous and differentiable for all r. R is usually chosen to include only the first neighbour shell. The repulsive and attractive terms f_R and f_A is modelled as an exponetial function, similar to a morse potential,

$$f_R(r) = A \exp(-\lambda_1 r),$$
$$f_A(r) = -B \exp\left(-\lambda_2 r\right).$$

The novel feature of the model lies in modeling of the bond order b_{ij} which includes three-body interactions by summing over a third atom $k \neq i, j$ within the cut-off $r_{ik} < R + D$ as shown in the following.

$$b_{ij} = \left(1 + \beta^n \zeta_{ij}^n\right)^{-\frac{1}{2n}} \tag{1.4}$$

$$\zeta_{ij} = \sum_{k \neq i,j} f_C(r_{ik}) g\left(\theta_{ijk}\left(r_{ij}, r_{ik}\right)\right) \exp\left(\lambda_3{}^m \left(r_{ij} - r_{ik}\right)^m\right) \tag{1.5}$$

$$g(\theta) = \gamma_{ijk}\left(1 + \frac{c^2}{d^2} - \frac{c^2}{\left[d^2 + \left(\cos\theta - \cos\theta_0\right)^2\right]}\right). \tag{1.6}$$

In eq. (1.6) $\zeta_{i,j}$ is an effective coordination and $g(\theta)$ captures angle dependency as it is minimized at the equilibrium angle $\theta = \theta_0$.

The parameters used to model the graphene C-C bonds is summarized in table 1.2

Table 1.2: Parameters for the tersoff potential used for intermolecular interations in the graphene sheet

Parameter	Value	Description
m	3.0	Default (not used since $\lambda_3 = 0$)
γ	1.0	...
λ_3	0.0 Å^{-1}	...
c	3.8049×10^4	Strength of the angular effect
d	4.3484	Determines the "sharpness" of the angular dependency
$\cos(\theta_0)$	-0.57058	Cosine of the equilibrium angle
n	0.72751	Power law exponent for the bond order dependency
β	1.5724×10^{-7}	...
λ_2	2.2119 Å^{-1}	Decay of repulsion potential term
B	346.74 eV	Attractive potential term minimum at core ($r_{ij} = 0$).
R	1.95 Å	Center distance for cut-off
D	0.15 Å	Thickness of cut-off layers
λ_1	3.4879 Å^{-1}	Decay of repulsion potential term
A	1393.6 eV	Repulsion potential term at core ($r_{ij} = 0$)

1.2.5 LAMMPS

1.2.6 Integration

Solving newtons equations of motion

$$\ddot{x}(t) = \frac{F(x)}{m} \quad \rightarrow \quad \dot{x} = v(t), \;\; \dot{v}(t) = \frac{F(x(t))}{m}$$

Integration of newtons equations of motion (just like, Euler, Euler cromer and so on) and specify the verlet algorithm which is used in Lammps.

The forces (form the potential) is conservative so the energy should be conserved before applying the thermostat.

However small erros applied by the discrete integraiton algorithm we end up having an energy error. This is sensitive to time step.

1.2.6.1 Velocity Verlet

Make it explicit that $\Delta t^2 = (\Delta t)^2$ and relax notation on this point.

The velocity verlet algorithm can be derived by taken a number of taylor expansion. We begin by expanding the next step position vector $\mathbf{x}(t + \Delta t)$ around time t

$$\mathbf{x}(t + \Delta t) = \mathbf{x}(t) + \dot{\mathbf{x}}\Delta t + \frac{\ddot{\mathbf{x}}}{2}(\Delta t)^2 + \mathcal{O}((\Delta t)^3) \tag{1.7}$$

Similar we take the expansions of the next step velocity vector $\mathbf{v}(t + \Delta t)$ at time t

$$\mathbf{v}(t + \Delta t) = \mathbf{v}(t) + \dot{\mathbf{v}}(t)\Delta t + \frac{\ddot{\mathbf{v}}(t)}{2}(\Delta t)^2 + \mathcal{O}((\Delta t)^3) \tag{1.8}$$

By also taking the taylor expansion of $\dot{\mathbf{v}}(t + \Delta t)$ we can eliminate the *v̈cv* term in eq. (1.8) as done in the following.

$$\dot{\mathbf{v}}(t + \Delta t) = \dot{\mathbf{v}}(t) + \ddot{\mathbf{v}}(t)\Delta t + \mathcal{O}((\Delta t)^2)$$
$$\frac{\ddot{\mathbf{v}}(t)}{2}(\Delta t)^2 = \frac{\Delta t}{2}\Big(\dot{\mathbf{v}}(t + \Delta t) - \dot{\mathbf{v}}(t)\Big) + \mathcal{O}((\Delta t)^3)$$
$$\Downarrow$$
$$\mathbf{v}(t + \Delta t) = \mathbf{v}(t) + \dot{\mathbf{v}}(t)\Delta t + \frac{\Delta t}{2}\Big(\dot{\mathbf{v}}(t + \Delta t) - \dot{\mathbf{v}}(t)\Big) + \mathcal{O}((\Delta t)^3)$$
$$= \mathbf{v}(t) + \frac{\Delta t}{2}\Big(\dot{\mathbf{v}}(t) + \dot{\mathbf{v}}(t + \Delta t)\Big) + \mathcal{O}((\Delta t)^3) \tag{1.9}$$

By combining eq. (1.7) and eq. (1.9) while cleaning up the notation using $\mathbf{v} = \dot{\mathbf{x}}$ and $\mathbf{a} = \dot{\mathbf{v}}$ we get the final scheme

$$\mathbf{x}(t + \Delta t) = \mathbf{x}(t) + \mathbf{v}(t)\Delta t + \frac{\mathbf{a}(t)}{2}(\Delta t)^2 + \mathcal{O}((\Delta t)^3),$$
$$\mathbf{v}(t + \Delta t) = \mathbf{v}(t) + \frac{\mathbf{a}(t) + \mathbf{a}(t + \Delta t)}{2}\Delta t + \mathcal{O}((\Delta t)^3).$$

The scheme will give a local error of order $(\Delta t)^3$ corresponding to a global error of $(\Delta t)^2$. Lets descritize the time as $t_k = k * \Delta t$ with position $\mathbf{x}_k$ and velocity $\mathbf{v}_k$. At time t_k the acceleration is given $\mathbf{a}_k = F(\mathbf{x}_k)/m$. We get the implementation steps as follows

1. Calculate $\mathbf{x}_{k+1} = \mathbf{x}_k + \mathbf{v}_k\Delta t + \frac{F(\mathbf{x}_k)}{2m}(\Delta t)^2$

2. Evaluate $F(\mathbf{x}_{k+1})$

3. Calculate $\mathbf{v}_{k+1} = \mathbf{v}_k + \frac{F(\mathbf{x}_k)+F(\mathbf{x}_{k+1})}{2m}\Delta t$

It is sometimes expressed as the following. This is mathematically the same, but is it computaitonally more efficient?

$$\mathbf{r}_i(t + \delta t) = \mathbf{r}_i(t) + \mathbf{v}_i(t)\delta t + \frac{\mathbf{f}_i(t)}{2m_i}\delta t^2$$

$$\mathbf{v}_i(t + \delta t/2) = \mathbf{v}_i(t) + \frac{\delta t}{2}\frac{\mathbf{f}_i(t)}{m_i}$$

$$\mathbf{f}_i(t + \delta t) = \mathbf{f}_i\left(\mathbf{r}_i(t + \delta t)\right)$$

$$\mathbf{v}_i(t + \delta t) = \mathbf{v}_i(t + \delta t/2) + \frac{\delta t}{2}\frac{\mathbf{f}_i(t + \delta t)}{m_i}$$

Further they suggest this to be the most used algorithm

$$\mathbf{v}_i(t + \delta t/2) = \mathbf{v}_i(t) + \frac{\delta t}{2}\frac{\mathbf{f}_i(t)}{m_i}$$

$$\mathbf{r}_i(t + \delta t) = \mathbf{r}_i(t) + \mathbf{v}_i(t + \delta t/2)\delta t$$

$$\mathbf{f}_i(t + \delta t) = \mathbf{f}_i(\mathbf{r}_i(t + \delta t))$$

$$\mathbf{v}_i(t + \delta t) = \mathbf{v}_i(t + \delta t/2) + \frac{\delta t}{2}\frac{\mathbf{f}_i(t + \delta t)}{m_i}$$

Make sure to check this out.

1.2.7   Thermostats

Langevin thermostat

The Langevin equation is Newtons second law for a Brownian particle where the forces include a viscous drag force from surrounding fluid and a random force fluctuation form collisions with the fluid molecules.

We describe the statistical nature of the collisions by the central limit theorem. The total momentum change ΔP can be described by the sum of individual momentum transfer δP to the brownian particle from the molecular collision.

$$\Delta P = \sum_i^N \delta p_i$$

where $\langle \delta p \rangle = 0$ and $\langle \delta p^2 \rangle = \sigma^2$. When N is large the central limit theorem yields that the random variable ΔP has a gaussian distirbution with $\langle P \rangle = 0$ and $\langle \Delta P^2 \rangle = N\sigma^2$. If ΔP is the momentum change over a discrete time Δt such that $N \propto \Delta t$ the corresponding force $\Delta P/\Delta t$ will have a variance

$$\langle \tilde{F} \rangle = \frac{\langle \Delta P^2 \rangle}{\Delta t^2} \propto \frac{1}{\Delta t}.$$

In a computer simulation we need to pick a random force $\tilde{F}(t)$ from a Gaussian distribution every time-step Δt. These forces will not be correlated since we assume that Δt is larger than the correlation time for the molecular forces (or do we just neglect them?). We may thus write the correlation function as

$$\langle \tilde{F}(t)\tilde{F}(0) \rangle = \begin{cases} \frac{a}{\Delta t}, & |\Delta t| < \Delta t/2 \\ 0, & |\Delta t| > \Delta t/2 \end{cases}$$

In the limit $\Delta t \to 0$ the correlation function becomes

$$\langle \tilde{F}(t)\tilde{F}(0)\rangle = a\delta(t-0) \tag{1.10}$$

This is valid for all spatial components (maybe make a point out of this). Since $\langle \tilde{F}\rangle = 0$ the random force (fluctuating force) will not conribute with a average decay (change) to the velocity. The macroscopic decay comes from the friction force (dissipitative force) $-ma = \alpha v$ (give variable explanation).

A version of newtons 2. law that combines these fluctuation forces and drag forces is the Langevin equation

$$m\dot{v} = -\alpha v + \tilde{F}$$

Both forces arises from the molecular fluid where the drag force represents the velocity dependence while the random force is taken to be velocity independent, i.e. $\langle F_i v_j\rangle = 0$ where i and j are cartesian indices. From the langevin equations we can compute the velocity (auto)correlation function. We do this in one dimension for simplicity. We multiply by $(e^{\alpha t/m})/m$

$$\dot{\mathbf{v}}(t)e^{\alpha t/m} + \frac{\alpha}{m}\mathbf{v}(t)e^{\frac{\alpha t}{m}} = \frac{\mathbf{F}}{m}e^{\frac{\alpha t}{m}},$$

and integrate from $t = -\infty$. By the use of integration by parts on latter term in the left hand side we calculate the velocity

$$\int_{-\infty}^{t} dt'\ \dot{\mathbf{v}}(t')e^{\frac{\alpha t'}{m}} + \frac{\alpha}{m}\mathbf{v}(t)e^{\frac{\alpha t'}{m}} = \int_{-\infty}^{t} dt'\ e^{\frac{\alpha t'}{m}}\frac{\mathbf{F}(t')}{m}$$

$$\int_{-\infty}^{t} dt'\ \dot{\mathbf{v}}(t')e^{\frac{\alpha t'}{m}} + \left(\left[\mathbf{v}(t')e^{\frac{\alpha t'}{m}}\right]_{-\infty}^{t} - \int_{-\infty}^{t} dt'\ \dot{\mathbf{v}}(t')e^{\frac{\alpha t'}{m}}\right) = \int_{-\infty}^{t} dt'\ e^{\frac{\alpha t'}{m}}\frac{\mathbf{F}(t')}{m}$$

$$\mathbf{v}(t) = \int_{-\infty}^{t} dt'\ e^{\frac{-\alpha(t-t')}{m}}\frac{\mathbf{F}(t')}{m},$$

where $e^{\frac{-\alpha t}{m}}$ plays the role of a response function (?). We can then calculate the autocorrelation

$$\langle \mathbf{v}(t)\mathbf{v}(0)\rangle = \int_{-\infty}^{t} dt_1\ \int_{-\infty}^{0} dt_2\ e^{\frac{t-t_1-t_2}{m}}\frac{\langle \mathbf{F}(t_1)\mathbf{F}(t_2)\rangle}{m^2}$$

$$= \int_{-\infty}^{t} dt_1\ \int_{-\infty}^{0} dt_2\ e^{\frac{t-t_1-t_2}{m}}\frac{a\delta(t_1-t_2)}{m^2}$$

$$= \int_{-\infty}^{0} dt_2\ e^{\frac{t-2t_2}{m}}\frac{a}{m^2} = \frac{a}{2m\alpha}e^{-\frac{\alpha t}{m}}$$

where we used eq. (1.10) and that the integration commutes with the average (we can change the order of integration). By comparing this with the equipartition theorem we get

$$\frac{1}{2}m\langle \mathbf{v}^2\rangle = \frac{k_B T}{2}$$

$$\frac{1}{2}m\langle \mathbf{v}(0)\mathbf{v}(0)\rangle = \frac{k_B T}{2}$$

$$\frac{a}{4\alpha} = \frac{k_B T}{2}$$

$$a = 2\alpha k_B T$$

We notice that α appears that the magnitude of the fluctuations increase both with friction and temperature.

This section is based on [15], [16](pp. 115, 120-121) and [17]

"The Langevin equation is Newtons second law for a Brownian particle, where the forces include both the viscous drag due to the surrounding fluid and the fluctuations caused by the individual collisions with the fluid molecules."

"Another option to simulate a system in the NVT ensemble is to use a stochastic thermostat, as opposed to the deterministic thermostat defined through the Nose-Hoover equations."

"The equations of mo- tion of a system with a stochastic thermostat are known as Brownian dynamic equations"

In order to simulate the canonical ensemble, that is the ensemble defined by a constant amount of particles N, constant temperature T and constant volume V, hence often denoted NVT, we apply a so-called thermostat. There exist a variety of such including Nosé-Hoover, Gaussian, Berendsen, Langevin thermostat and many other (give example of how they modify) We will use the ladder.

The connical ensemble is an ensemble of systems by the assumption that the system of interests is connected to an infitely large heat bath of temperature T. The Langevin thermostat assumes that the particles collides with much smaller lighter particles representing the heat bath as a sea of small particles. The collisions is described by a friction force $f_f = -\gamma\mathbf{p}$, where γ is positiv friction coefficient and $\mathbf{p}$ the momentum vector, and a random force $f_r = \mathbf{R}_i(t)$. By denoting the conservative force arising from the usual inter-particle interactions $\mathbf{f}_i$ on particle i we get the Langevin equations of motion describing the total force $\mathbf{F}_i$ on particle i as

$$\mathbf{F}_i = \mathbf{f}_i + \mathbf{f}_{f,i} + \mathbf{f}_{r,i}$$
$$m_i\ddot{\mathbf{r}}_i = \mathbf{f}_i - \gamma_i\mathbf{p}_i + \mathbf{R}_i(t) \tag{1.11}$$

where m_i is the mass of particle i $\mathbf{r}_i$ the position vector. The random force $\mathbf{R}_i(t)$ is described as gaussian white noise and have the following properties.

1. It is uncorrelated with the velocities $\dot{\mathbf{r}}(t)$ and deterministic forces $\mathbf{f}_i(t')$ at previous times $t' < t$.

2. The time average is zero: $\langle\mathbf{R}(t)\rangle = \mathbf{0}$.

3. The mean-square components evaluate to $2m_i\gamma_i k_B T$.

4. The force component of particle i $R_{i,\mu}$ along cartesian axis μ is uncorrelated with any component of particle j $R_{i,\nu}$ along cartesian axis ν, unless $i = j$, $\mu = \nu$ and $t = t'$.

The ladder two conditions can be formulated as

$$\langle R_{i,\mu}(t)R_{j,\nu}(t')\rangle = 2m_i\gamma_i k_B T\delta_{ij}\delta_{\mu\nu}\delta(t' - t),$$

where $\delta_{..}$ is the Kronecker Delta function and $\delta(\cdot)$ is the Dirac Delta function. It can be shown that a trajectory generated by integrating the Langevin equations of motion (eq. (1.11)) maps a cononical distribution of microstates at temperature T. [16](p.121). (Can I say something more about the relationship between the friction froce and the random force - How to the balance to give NVT. Is the proof complicated?)

In practice the implementation of the thermostat is implemented discretely by updating the force on each particle by the addition of the described forces f_f and f_r for each particle. In LAMMPS this is controlled by the user defined damping factor "damp" $= \gamma^{-1}$ in units of time whih control how fast we are going to reach the temperature equlibrium. Thus the documentation ([17]) defines the added forces as

$$f_f = -\frac{m}{\text{damp}}, \qquad f_r \propto \sqrt{\frac{mk_B T}{dt\,\text{damp}}}$$

where $v = [\dot{r}]$ is the velocity. The definition of f_f falls straight out of the definition above in eq. (1.11) while the proportionality of f_r comes from

$$\sqrt{\langle R(t)^2 \rangle} = \sqrt{2m\gamma k_B T} \propto \sqrt{\frac{mk_B T}{\text{damp}}}$$

Thus we have $f_r \propto \sqrt{\langle R(t)^2 \rangle / dt}$ which I do not quite understand. It is mentioned in https://pubs.acs.org/doi/full/10.1021/ct8002173 when talkikng about residual forces, as it is natural when taking a step length of dt... Probably simply, but check this later.
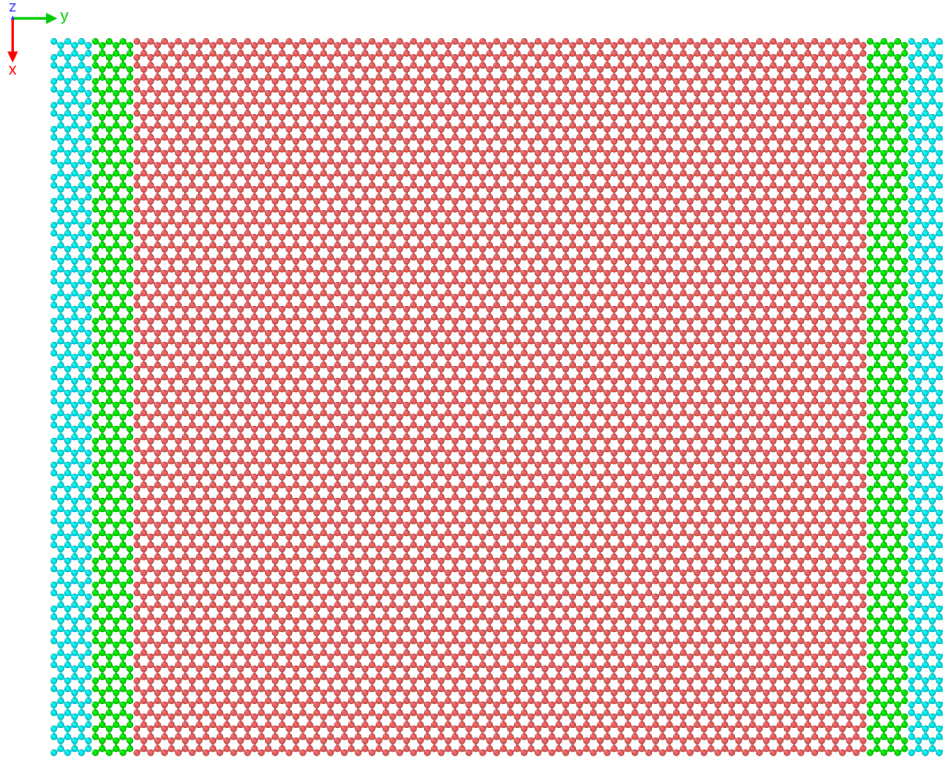
1.3 Defining the system

1.3.1 Groups: Sheet, pullblocks and substrate

Include figure of system to point out thermo layers and freeze layers.
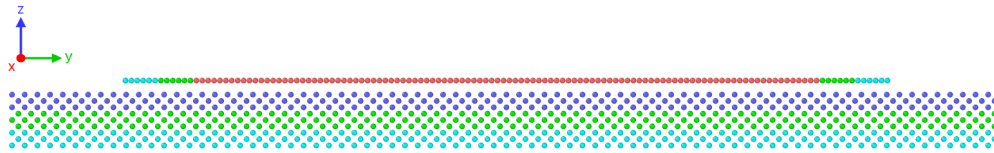
(a) Side view

(b) Top view

Figure 1.1: System. 27456 atoms in total: 7272 with thermostat (orange), 7272 is locked (light blue) and the remaing 12912 just with NVE. (Get better colors)

Table 1.3: System atom count and region division.

Region	Total	Sub region	Sub total	NVE	NVT	Locked
Sheet	7800	Inner sheet	6360	6360	0	0
		Pull blocks	1440	0	720	720
Substrate	19656	Upper	6552	6552	0	0
		Middle	6552	0	6552	0
		Bottom	6552	0	0	6552
All	27456			12912	7272	7272

1.3.2   Creating sheets

We are going to create a 2D sheet graphene sheet.

1.3.2.1   Graphene

Graphene is a single layer of carbon atom, graphite is the bulk, arranged in a hexagonallattice structure. We can describe the 2D crystal structure in terms of its primitive lattice vector and a basis. That is we populate each lattice site by the given basis and translate it to fill the whole plane by any linear combination of the lattice vectors

$$\mathbf{T}_{mn} = m\mathbf{a_1} + n\mathbf{a_2}, \qquad m, n \in \mathbb{N}.$$

For graphene we have the primitive lattice vectors

$$\mathbf{a_1} = a\left(\frac{\sqrt{3}}{2}, -\frac{1}{2}\right), \qquad \mathbf{a_2} = a\left(\frac{\sqrt{3}}{2}, \frac{1}{2}\right), \qquad |\mathbf{a_1}| = |\mathbf{a_2}| = 2.46 \text{ Å}.$$

Notice that we deliberately excluded the third coordinate as we only consider a single graphene layer on not the bulk graphite consisting of multiple layers stacked on top of each other. The basis is

$$\left\{ \left(0, 0\right), \frac{a}{2}\left(\frac{1}{\sqrt{3}}, 1\right) \right\}$$

It turns out that the spacing between atoms is equal for all paris with an interatomic distance

$$\left| \frac{a}{2}\left(\frac{1}{\sqrt{3}}, 1\right) \right| \approx 1.42 \text{ Å}.$$
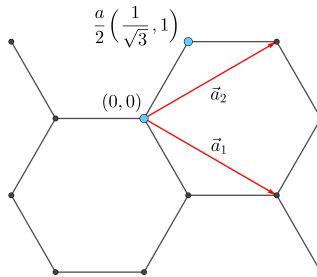
Figure 1.2: Graphene crystal structure with basis.

1.3.2.2 Indexing

In order to define the cut patterns applied to the graphene sheet we must define an indexing system. We must ensure that this gives an unique description of the atoms as we eventually want to pass a binary matrix, containg 0 for removed atom and 1 for present atom, that uniquely describes the sheet. We do this by letting the x-coordinate point to zigzag chains and the y-coordinate to the position along that chain. This is illustrated in figure 1.3. Other solutions might naturally invole the lattice vectors, but as these only can be used to translate to similar basis atoms a unfortunate duality is introduced as ones need to include the basis atom of choice into the indexing system. With the current system we notice that locallity is somewhat preserved. That is, atom (i,j) is in the proximity of $\{(i+1,j),(i-1,j),(i,j+1),(i,j-1)\}$, but only three of them is categorized as nearest neighbours due to the hexgonal structure of the lattice. While $(i,j\pm1)$ is always nearest neighbours the neighbour in the x-direction flip sides with incrementing y-coordinate. That is the nearest neighbours (NN) is decided as

$$j \text{ is even} \rightarrow \text{NN} = \{(i+1,j),(i,j+1),(i,j-1)\},$$
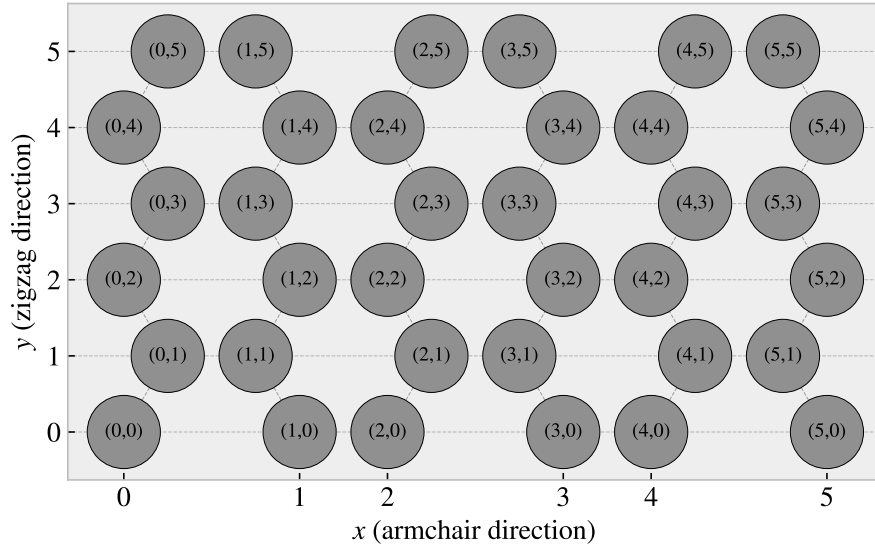$$j \text{ is odd} \rightarrow \text{NN} = \{(i-1,j),(i,j+1),(i,j-1)\}.$$

Figure 1.3: Graphene atom indexing

1.3.2.3 Removing atoms

As a mean to ease the formulation of cut patterns we introduce pseudo center element in each gap of the hexagonal honeycombs, see figure 1.4.
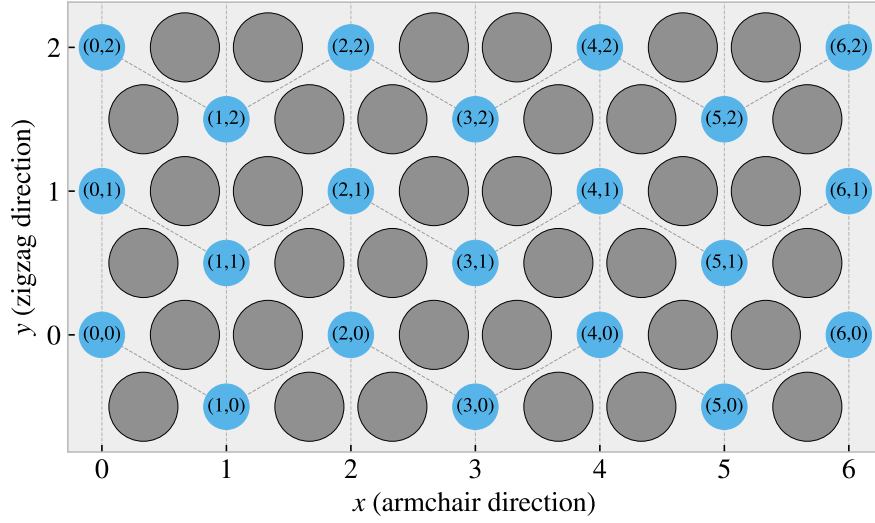
Figure 1.4: Graphene center indexing

Similar to the case of the indexing for the carbon atoms themself the nearest neighbour center elements alternate with position, this time along the x-coordinate. Each center element has six nearest neighbours, in clock wise direction we can denote them: "up", "upper right", "lower right", "down", "lower left", "upper left". The "up" and "down" is always accesed as $(i, j \pm 1)$, but for even i the $(i+1, j)$ index corresponds to the "lower right" neighbour while for odd i this corresponds to the "upper right" neighbour. This shifting applies for all left or right neighbours and the full neighbour list is illustrated in figure 1.5.
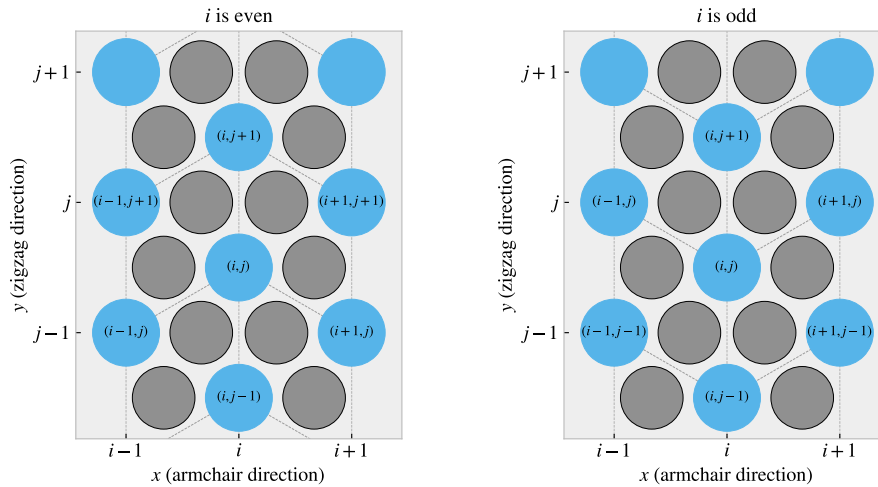

Figure 1.5: Graphene center elements directions

We define a cut pattern by connecting center elements into connected paths. As we walk element to element we remove atoms according to one of two rules

1. Remove intersection atoms: We remove the pair of atoms placed directly in the path we are walking. That is, when jumnping to the "up" center element we remove the two upper atoms located in the local hexagon of atoms. This method is sensitive to the order of the center elements in the path.

2. Remove all surrounding atoms: We simply remove all atoms in the local hexagon surrounding each center element. This method is indepdent of the ordering of center elements in the path.

We notice that removing atoms using either of these rules will not garuantee an unique cut pattern. Rule 1 is the more sensitive to paths but we realize that, for an even i, we will remove the same five atoms following

either of the following paths.

$$(i, j) \rightarrow \underbrace{(i+1, j+1)}_{\text{upper right}} \rightarrow \underbrace{(i, j+1)}_{\text{up}} \rightarrow \underbrace{(i+1, j+2)}_{\text{upperright + up}} \rightarrow \underbrace{(i+1, j+1)}_{\text{upper right}}$$

$$(i, j) \rightarrow \underbrace{(i+1, j+1)}_{\text{upper right}} \rightarrow \underbrace{(i+1, j+2)}_{\text{upperright + up}} \rightarrow \underbrace{(i, j+1)}_{\text{up}}$$

For rule 2 it is even more abovious that different paths can result in the same atoms being removed. This is the reason that we needed to define and indexing system for the atom position itself even though that all cuts generated manually will use the center element path as reference.

Illustrate some delete path?

1.3.3 Pull blocks

1.3.4 Kirigami inspired cut out patterns

1.3.4.1 Pop-up pattern

1.3.4.2 Honeycomb

1.3.4.3 Random walk

1.4 Fourier Transform (light)

Find out where to put this if nessecary.

Fourier transform is a technique where we transform a function $f(t)$ of time to a function $F(k)$ of frequency. The Forward Fourier Transform is done as

$$F(k) = \int_{-\infty}^{\infty} f(t)e^{-2\pi i k x} dx$$

For any complex function $F(k)$ we can decompose it into magnitude $A(k)$ and phase $\phi(k)$

$$F(k) = A(k)e^{i\phi(k)}$$

Hence when performing a Forward Fourier transform on a time series we can determine the amplitude and phase as a function of freqeuncy as

$$A(k) = |F(k)|^2, \qquad \phi(k) = \Im \ln F(k)$$

1.4.1 Real life experimental procedures

From Introduction to Tribology, Second Edition, p. 526:
    The surface force apparatus (SFA), the scanning tunneling microscopes (STM), and atomic force and friction force microscopes (AFM and FFM) are widely used in nanotribological and nanomechanics studies.

- Real life procedures to mimic in computation, for instance Atomic Force Microscoopy (AFM) for friction measurements.

- Available technology for test of my findings if successful (possibilities for making the nano machine)

1.5   Machine Learning (ML)

- Feed forward fully connected

- CNN

- GAN (encoder + decoder)

- Genetic algorithm

- Using machine learning for inverse designs partly eliminate the black box problem. When a design is produced we can test it, and if it works we not rely on machine learning connections to verify it's relevance.

- However, using explanaitons techniques such as maybe t-SNE, Deep dream, LRP, Shapley values and linearizations, we can try to understand why the AI chose as it did. This can lead to an increased understanding of each design feature. Again this is not dependent on the complex network of the network as this can be tested and veriied independently of the network.

1.5.1   Feed forward network / Neural networks

1.5.2   CNN for image recognition

1.5.3   GAN (encoder + deoder)

1.5.4   Inverse desing using machine learning

1.5.5   Prediction explanation

1.5.5.1   Shapley

1.5.5.2   Lineariations

1.5.5.3   LRP

1.5.5.4   t-SNE

Bibliography

[1] E. Gnecco and E. Meyer, *Elements of Friction Theory and Nanotribology.* Cambridge University Press, 2015, 10.1017/CBO9780511795039.

[2] J. H. Dieterich, *Time-dependent friction in rocks*, *Journal of Geophysical Research (1896-1977)* **77** (1972) 3690–3697, [https://agupubs.onlinelibrary.wiley.com/doi/pdf/10.1029/JB077i020p03690].

[3] H.-J. Kim and D.-E. Kim, *Nano-scale friction: A review*, .

[4] Y. Mo, K. T. Turner and I. Szlufarska, *Friction laws at the nanoscale*, .

[5] N. Manini, G. Mistura, G. Paolicelli, E. Tosatti and A. Vanossi, *Current trends in the physics of nanoscale friction*, *Advances in Physics: X* **2** (may, 2017) 569–590.

[6] S. Li, Q. Li, R. W. Carpick, P. Gumbsch, X. Z. Liu, X. Ding et al., *The evolving quality of frictional contact with graphene*, .

[7] J. Tersoff, *New empirical approach for the structure and energy of covalent systems*, *Phys. Rev. B* **37** (Apr, 1988) 6991–7000.

[8] S. Corporation, "pair_style lj/cut command."

[9] X. Wang, S. Ramírez-Hinestrosa, J. Dobnikar and D. Frenkel, *The lennard-jones potential: when (not) to use it*, *Phys. Chem. Chem. Phys.* **22** (2020) 10624–10633.

[10] R. Naeem, "Lennard-jones potential."

[11] Q. Zhang, D. Diao and M. Kubo, *Nanoscratching of multi-layer graphene by molecular dynamics simulations*, *Tribology International* **88** (2015) 85–88.

[12] S. Corporation, "pair_style sw command."

[13] F. H. Stillinger and T. A. Weber, *Computer simulation of local order in condensed phases of silicon*, *Phys. Rev. B* **31** (Apr, 1985) 5262–5271.

[14] S. Corporation, "pair_style tersoff command."

[15] T. Schneider and E. Stoll, *Molecular-dynamics study of a three-dimensional one-component model for distortive phase transitions*, *Phys. Rev. B* **17** (Feb, 1978) 1302–1322.

[16] P. H. Hünenberger, *Thermostat Algorithms for Molecular Dynamics Simulations*, pp. 105–149. Springer Berlin Heidelberg, Berlin, Heidelberg, 2005. 10.1007/b99427.

[17] S. Corporation, "fix langevin command."